A Compressive Sensing Based Colocated MIMO Radar Power Allocation and Waveform Design

Abdollah Ajorloo, *Student Member, IEEE,* Arash Amini, *Senior Member, IEEE,* and Mohammad Hassan Bastani

***Abstract*—Compressive Sensing (CS) is a widely used technique for (multiple) target detection in MIMO radars. In this work, our goal is to enhance the quality of CS-based detection techniques for a colocated MIMO radar with given location of transmit and receive nodes. Our approach is to design the transmit waveforms based on the given antenna locations, and optimally allocate the total power budget among the transmitters. The design criterion in this work is the coherence of the resulting sensing matrix. Based on this criterion, we derive and solve a convex optimization problem for power allocation. For waveform design, however, the direct method studied in [2] is non-convex, and although iterative descent methods could be used to achieve suboptimal solutions, they might be unfeasible waveforms (e.g. waveforms with high peak to average power ratios). Here, we first show that the coherence measure depends only on the covariance matrix of the waveforms (rather than the waveforms themselves). Next, we introduce three different convex programs to achieve the covariance matrix. Finally, we transform the covariance matrix into realistic waveforms; although multiple solutions exist, a closed-form expression for all possible solutions is available. Specifically, we design the waveforms by applying practical constraints such as constant modulus. Simulation results confirm that the introduced designs improve the detection performance of a CS-MIMO radar.**

***Index Terms*—Coherence measure, Compressive sensing, MIMO radar, Power allocation, Waveform design.**

I. Introduction

AMONG radar systems, MIMO radars have attracted a lot of attention in recent years [3]–[6]. This popularity is partly motivated by the fact that a MIMO radar consists of multiple transmit (TX) and receive (RX) antennas, where there is considerable freedom in the placement of the antennas and the transmitting signals. Antenna configuration in a MIMO radar system can be either colocated [5] or widely separated [4]. In a widely separated MIMO radar, antennas are far from each other compared to the distance to the targets. Hence, they view a given target with different angles and possibly different reflection coefficients. This property is commonly described as spatial diversity, which could significantly improve the detection performance in ideal setups. In contrast, the antennas of a colocated MIMO radar are closely spaced such that they all view the targets with almost the same angle and reflection coefficient. To compensate for the spatial diversity, a colocated MIMO radar exploits waveform diversity which improves parameter identifiability, interference rejection and spatial resolution. Therefore, the waveforms play a crucial role in the performance of colocated MIMO radars and their design has been studied in various works such as [7]–[13]. The more common approach in waveform design for colocated MIMO radars is to focus on the beam-pattern; in this work, however, we study power allocation and waveform design from the perspective of compressive sensing (CS). In other words, we consider CS-based colocated MIMO radars which exhibit outstanding detection performance.

Due to multiple transmit-receive channels, the signal model in a MIMO radar system is usually described by high-dimensional data structures. However, the desired target space (e.g. range-Doppler domain) which shall be estimated, is mainly sparse (the number of existing targets is usually small). This observation has promoted the use of sparse recovery methods in multi-target detection and estimation in MIMO radar systems. The application of sparse modeling to MIMO radars has been adressed both for colocated MIMO radars (e.g. in [14]–[17]) and widely separated MIMO radars (e.g. in [18]–[20]). In both cases, a sparse representation is considered for the targets in the target space and the estimation of targets is performed via sparse recovery methods studied in the field of compressed sensing.

The results in compressed sensing imply that a K-sparse vector $\mathbf{x}_{N\times 1}$ that consists of at most K nonzero elements ($K \ll N$), can be recovered from $M < N$ noisy linear measurements $\mathbf{y}_{M\times 1} = \mathbf{\Psi}\mathbf{x}+\mathbf{n}$, if the sensing matrix $\mathbf{\Psi}_{M\times N}$ is well-behaved. It is standard to invoke the so-called restricted isometry property (RIP) for $\mathbf{\Psi}_{M\times N}$ [21].

Although RIP is a strong sufficient condition for stable recovery, it is an NP-hard problem to verify it for a specific matrix $\mathbf{\Psi}_{M\times N}$.In deterministic scenarios where a $\mathbf{\Psi}_{M\times N}$ is given (or dictated by the physics of the problem), it is common to evaluate the coherence of the matrix:

$$\mu(\mathbf{\Psi}) = \max_{l\neq l'} \frac{|\boldsymbol{\psi}_{l'}^H \boldsymbol{\psi}_l|}{\|\boldsymbol{\psi}_{l'}\|_2 \|\boldsymbol{\psi}_l\|_2}, \tag{1}$$

where $\boldsymbol{\psi}_i$ stands for the ith column of $\mathbf{\Psi}$. It is well-known that a matrix with coherence $\mu(\mathbf{\Psi}) \leq \frac{\alpha}{2K-1}$ and $\alpha < 1$ satisfies RIP of order $2K$ (required for K-sparse signal recovery) [22]. Although this RIP bound is rather conservative, it shows that matrices with small coherence automatically satisfy RIP. Furthermore, evaluating the coherence value of an $M \times N$ matrix requires $\mathcal{O}(M\,N^2)$ operations which is polynomial and computationally feasible. For design purposes, it is desirable to keep $\mu(\mathbf{\Psi})$ as small as possible.

The authors are with the Electrical Engineering department at Sharif university of technology, Tehran, Iran, e-mail: ajorloo@ee.sharif.edu, aamini@sharif.ir, bastani@sharif.ir

Manuscript received xx xx, 2017; revised xx xx, 2015.

A related work with around 50% overlap with Section III of the current work was previously presented at EUSIPCO2017 and was published in the procedeeing [1]. It is available at http://ieeexplore.ieee.org/abstract/document/8081545.

Improving the performance of sparse recovery techniques by reducing the coherence of the sensing matrix in CS-based radars, and especially in CS-based MIMO radars, has been studied in some of the previous works such as [2], [16], [23]–[25]. In CS-based MIMO radars, power allocation and waveform design can be exploited as degrees of freedom to reduce the coherence [2], [16], [25]. Waveform design in CS-based MIMO radars was also studied in [26], [27], but not with the goal of coherence reduction.

A. Related Works

Waveform design in CS-based SISO radars was approached in [23], [24] by indirectly minimizing the coherence of the sensing matrix. In particular, in [24] the Gram matrix $\mathbf{\Psi}^H\mathbf{\Psi}$ is expressed in terms of the tunable parameters (e.g. waveform samples), and using an iterative method, the cost $\|\mathbf{\Psi}^H\mathbf{\Psi}-\mathbf{I}\|_F$ is minimized. This cost roughly represents the ℓ_2-norm of the off-diagonal elements of $\mathbf{\Psi}^H\mathbf{\Psi}$, while the ℓ_∞-norm determines the coherence value of $\mathbf{\Psi}$. In [16] which is one of the primary works on CS-based MIMO radars in the colocated setting, the problem of waveform design with the aim of coherence minimization along with the beam-pattern design has been considered; in this setting, uniform linear arrays are considered for TX and RX antennas. Instead of the standard coherence definition of (1), [16] employs the unnormalized version of the form $\widetilde{\mu}(\mathbf{\Psi}) = \max_{l\neq l'} |\boldsymbol{\psi}_{l'}^H\boldsymbol{\psi}_l|$. The minimization of the latter coherence form is also conducted using the simulated annealing algorithm of [16], which leads to a suboptimal solution in general. In [25], a CS-based colocated MIMO radar with frequency hopping waveforms is studied where the waveform design problem is reduced to a frequency code selection scheme. Then, a block coherence criterion is iteratively minimized to perform the selection. In [2], the power allocation problem for the widely-separated setting, and both power allocation and waveform design problems for the colocated setting are addressed. By adopting the proposed configuration of [15] in the colocated setting, the TX and RX antennas of the MIMO radar are assumed to be the nodes of a small-scale wireless sensor network that are randomly located in a disk of a small radius. For improving the estimation of the direction of arrivals (DOA) of the targets in the azimuth space, the search for a Gram matrix $\mathbf{\Psi}^H\mathbf{\Psi}$ as close as possible (in the ℓ_2 sense) to the identity matrix is devised in both power allocation and waveform design problems. Again this metric approximates but not equals the coherence value. By assuming the orthogonality of the transmitted waveforms, the mentioned minimization in the power allocation problem is convex; however, it is non-convex in the waveform design scenario and only a suboptimal solution via iterative methods (with possibly large computational cost) is achievable.

B. Contributions

In this paper, we consider the same model as in [2] and consider the power allocation and waveform design problems. For power allocation, adopting a set of orthogonal transmitted waveforms, we consider the exact coherence value of the sensing matrix (according to (1)) as the cost function and derive a convex optimization problem to minimize it. For designing the waveforms, we first show that the coherence value is solely determined by the covariance matrix of the transmitted waveforms. Next, we introduce a convex program to obtain the optimal covariance matrix. Fortunately, there are infinitely many sets of waveforms with the same covariance matrix; this gives us some degrees of freedom in selecting a set of optimal waveforms. For instance, among the optimal solutions, one might seek the set that better suits practical considerations such as having constant modulus waveforms or waveforms with low peak-to-average-power ratios (PARs). It should be noted that all existing methods, especially the one proposed in [2] focus on determining the waveforms directly and ignore the fact that multiple sets of optimal solutions might exist. For obtaining the optimal covariance matrix, we derive three different convex programs that can be efficiently solved using packages such as CVX [28]; numerical simulations confirm that the proposed methods have considerably less computational time compared to the iterative method of [2]. For extracting the waveforms from the achieved covariance matrix, we follow the method of [10] to synthesize waveforms with constant modulus property.

The rest of the paper is organized as follows. The signal model and the mathematical formulation of received signals is discussed in Section II. The proposed power allocation and waveform design schemes are presented in Section III and section IV, respectively. Our numerical tests that confirm the performance of the proposed methods are given in Section V. Finally, we conclude the paper in Section VI.

II. Signal Model

In this paper, we consider a MIMO radar with the same configuration as in [15] and [2]. More specifically, we assume M transmitters and N receivers that are randomly located in a small area (a small-scale sensor network) which form a colocated MIMO radar. In polar coordinates, the location of TX and RX nodes are denoted by (r_i^t, α_i^t) and (r_i^r, α_i^r), respectively. RX nodes, after receiving and sampling the scattered signals from the targets, send the samples to a fusion node that combines all the collected data, and detects the targets. To mathematically describe the radar signals, let us denote the matrix of the transmitted waveforms in baseband by $\mathbf{X}_{L\times M}$, where each column corresponds to a transmitter and rows encode the time instances. Under far-field assumption, the normalized (with respect to the origin) transmit steering vector at azimuth angle θ denoted by $\mathbf{a}_{M\times 1}(\theta)$, is given by

$$\mathbf{a}(\theta) = [\mathrm{e}^{\mathrm{j}\frac{2\pi}{\lambda}d_1^t(\theta)}, \mathrm{e}^{\mathrm{j}\frac{2\pi}{\lambda}d_2^t(\theta)}, \ldots, \mathrm{e}^{\mathrm{j}\frac{2\pi}{\lambda}d_M^t(\theta)}]^T, \qquad (2)$$

where $d_i^t(\theta) = r_i^t\cos(\theta-\alpha_i^t)$. If there are K targets in the far-field of the radar at azimuth angles $\{\theta_k\}_{k=1}^K$ and at approximately the same range (common simplifying assumption), the received signal at the ith RX node in the baseband form can be approximated by

$$\mathbf{r}_i = \sum_{k=1}^{K} \beta_k \mathrm{e}^{\mathrm{j}\frac{2\pi}{\lambda}d_i^r(\theta_k)}\,\mathbf{X}\,\mathbf{a}(\theta_k) + \mathbf{n}_i, \qquad (3)$$

where β_ks are complex coefficients proportional to RCSs of the targets, $d_i^r(\theta) = r_i^r \cos(\theta - \alpha_i^r)$, and $\mathbf{n}_i$ stands for the additive noise vector at the ith receiver which is modeled by a circularly symmetric complex Gaussian random vector with variance σ^2.

The azimuth angle of each target is generally a real number. In practice, however, due to quantization and other resolution-limiting factors, the estimated angles by the radar have finite precision and belong to a finite set. In other words, there are finitely many azimuth angles possible as the output of the radar. Here, we assume the set of output angles of the radar form a grid with linearly spaced azimuth angles $\gamma_1, \gamma_2, \ldots, \gamma_{N_g}$. Moreover, the grid is fine enough that the error of the nearest-neighbor map from the exact azimuth angles of the targets to this set is tolerable. Thus, in the rest of the paper we only consider the case where the target angles belong to the grid. This way, the received signal at the ith RX node can be expressed as

$$\mathbf{r}_i = \mathbf{\Psi}_i \mathbf{s} + \mathbf{n}_i, \tag{4}$$

where

$$\mathbf{\Psi}_i = [\mathrm{e}^{\mathrm{j}\frac{2\pi}{\lambda} d_i^r(\gamma_1)} \mathbf{X}\mathbf{a}(\gamma_1), \ldots, \mathrm{e}^{\mathrm{j}\frac{2\pi}{\lambda} d_i^r(\gamma_{N_g})} \mathbf{X}\mathbf{a}(\gamma_{N_g})] \tag{5}$$

is regarded as the sensing matrix of the ith receiver, and $\mathbf{s} = [s_1, s_2, \ldots, s_{N_g}]$ is the K-sparse vector of target's reflection coefficients ($N_g \gg K$); the non-zero elements occur only at the corresponding location of the targets. Since the radar is colocated, the vector $\mathbf{s}$ is the same for all $1 \le i \le N$.

If we stack all the received vectors from RX nodes at the fusion node to obtain $\mathbf{r}$, we can write that

$$\mathbf{r} = [\mathbf{r}_1^T, \ldots, \mathbf{r}_N^T]^T = \underbrace{[\mathbf{\Psi}_1^T, \ldots, \mathbf{\Psi}_N^T]^T}_{\mathbf{\Psi}} \mathbf{s} + \underbrace{[\mathbf{n}_1^T, \ldots, \mathbf{n}_N^T]^T}_{\mathbf{n}}. \tag{6}$$

This suggests that $\mathbf{s}_{N_g \times 1}$ could be found as the sparse solution of (6) with $\mathbf{\Psi}_{NL \times N_g}$ and $\mathbf{n}_{NL \times 1}$ being the overall sensing matrix and noise vector, respectively. The literature is quite rich in sparse recovery methods; provided that $\mathbf{s}$ is sparse enough, it can be estimated using a variety of sparse recovery methods such as [29]–[32]. As we frequently deal with complex-valued vectors and matrices, we use NESTA proposed in [32] for the recovery of sparse vectors in this paper. In the noiseless case, the support of the recovered sparse vector determines the location of the targets. In the noisy case, however, we compare the amplitude of the elements of the recovered vector with a pre-determined threshold to decide about the presence of a target at a given angle. The threshold itself is determined by a constant false alarm rate (CFAR) strategy.

A minor but practical point is that the sparse recovery formulation in (6) is applicable if all the sensor nodes are synchronized when transmitting their data to the fusion node and the location of TX/RX nodes are available at the fusion node.

III. Power Allocation

As mentioned in Section I, our design approach is to minimize the coherence of the overall sensing matrix. Obviously, smaller coherence values lead to stronger recovery guarantees for sparse signals.

We recall that the matrix $\mathbf{X}$ contains all the transmitting signals, which automatically includes the transmitting power of each TX node. To separately discuss the role of power and waveform in our design, we assume the columns of $\mathbf{X}$ have unit norm and consider the amplification factors separately. More specifically, we represent the lth column of the overall sensing matrix $\mathbf{\Psi}$ with $\mathbf{u}_l$ as

$$\mathbf{u}_l = \mathbf{b}(\gamma_l) \otimes (\mathbf{X}\,\mathbf{A}(\gamma_l)\,\widehat{\mathbf{p}}), \tag{7}$$

where

$$\mathbf{b}(\gamma_l) = \left[\mathrm{e}^{\mathrm{j}\frac{2\pi}{\lambda} d_1^r(\gamma_l)}, \ldots, \mathrm{e}^{\mathrm{j}\frac{2\pi}{\lambda} d_N^r(\gamma_l)}\right]^T$$

is the receive steering vector at azimuth angle γ_l, $\otimes$ is the Kronecker product, $\widehat{\mathbf{p}}$ is the element-wise square-root of the power vector $\mathbf{p} = [p_1, \ldots, p_M]^T$ (p_i is the transmitting power of the ith TX node), and

$$\mathbf{A}(\gamma_l) = \mathrm{diag}\,\{\mathbf{a}(\gamma_l)\}.$$

In the power allocation problem, we assume that $\mathbf{X}$ with unit-norm columns is given, and we minimize the coherence of $\mathbf{\Psi}$ by tuning the transmitting powers at TX nodes (elements of the power vector $\mathbf{p}$, or alternatively, their square-roots in $\widehat{\mathbf{p}}$). Due to the complicated dependence of the optimal power values to the waveforms in $\mathbf{X}$, we further assume that the columns of $\mathbf{X}$ are pairwise orthogonal; i.e., TX nodes employ orthogonal waveforms. By combining the unit-norm and orthogonality assumptions, we conclude that $\mathbf{X}^H\mathbf{X} = \mathbf{I}$. With this result, the inner product of the columns l and l' of $\mathbf{\Psi}$ ($\mathbf{u}_l$ and $\mathbf{u}_{l'}$, respectively) simplifies to [2]

$$|\mathbf{u}_{l'}^H \mathbf{u}_l|^2 = b_{ll'}\, \mathbf{p}^T \big(\mathbf{c}_{ll'} \mathbf{c}_{ll'}^H\big) \mathbf{p}, \tag{8}$$

where

$$b_{ll'} = |\mathbf{b}^H(\gamma_{l'})\,\mathbf{b}(\gamma_l)|^2 = \Big| \sum_{n=1}^{N} \mathrm{e}^{\mathrm{j}\frac{2\pi}{\lambda}\left(d_n^r(\gamma_l) - d_n^r(\gamma_{l'})\right)} \Big|^2 \tag{9}$$

and $\mathbf{c}_{ll'}$ is the diagonal vector of $\mathbf{A}^H(\gamma_{l'})\,\mathbf{A}(\gamma_l)$ (note that $\mathbf{A}(\gamma_i)$s are diagonal matrices). By setting $l' = l$, we obtain $b_{ll} = N^2$ and $\mathbf{c}_{ll} = \mathbf{1}_{M \times 1}$; hence, the norm of the lth column of $\mathbf{\Psi}$ is given by

$$\|\mathbf{u}_l\|_2 = \Big(N \sum_{m=1}^{M} p_m\Big)^{0.5} = \sqrt{N}\, \|\mathbf{p}\|_1^{0.5}, \tag{10}$$

which is the same for all $l = 1, \ldots, N_g$. According to (8) and (10), the coherence of $\mathbf{\Psi}$ can be evaluated as

$$\mu(\mathbf{\Psi}) = \max_{l \neq l'} \frac{|\mathbf{u}_{l'}^H \mathbf{u}_l|}{\|\mathbf{u}_{l'}\|_2 \|\mathbf{u}_l\|_2} = \max_{l \neq l'} \frac{\sqrt{b_{ll'} \mathbf{p}^T (\mathbf{c}_{ll'} \mathbf{c}_{ll'}^H) \mathbf{p}}}{N\, \|\mathbf{p}\|_1}. \tag{11}$$

Equation (11) reveals that $\mu(\mathbf{\Psi})$ remains unchanged by uniformly scaling the power vector $\mathbf{p}$ (However the effective signal-to-noise ratio changes). This in turn shows that, rather than the total power budget ($\sum_{m=1}^{M} p_i$), the relative power values determine the coherence value. Therefore, to find the optimal power distribution, we fix the total power budget to a given value P_t (determined by limitations on energy

consumption). We also consider a per antenna maximum power constraint (P_m) and formulate the following problem.

$$\mathbf{p}_{\text{opt}} = \underset{\mathbf{p}}{\text{argmin}} \ \max_{l \neq l'} \ b_{ll'}\, \mathbf{p}^T(\mathbf{c}_{ll'}\mathbf{c}_{ll'}^H)\mathbf{p} \quad \text{s.t.} \begin{cases} \mathbf{1}_{M\times 1}^T \mathbf{p} = P_t, \\ \mathbf{p} \geq \mathbf{0}, \\ \mathbf{p} \leq P_m. \end{cases} \tag{12}$$

For all $l \neq l'$, as the scalar $b_{ll'}$ is a non-negative and the matrix $\mathbf{c}_{ll'}\mathbf{c}_{ll'}^H$ is a non-negative definite, the function $b_{ll'}\, \mathbf{p}^T(\mathbf{c}_{ll'}\mathbf{c}_{ll'}^H)\mathbf{p}$ is convex with respect to $\mathbf{p}$. Consequently, $\max_{l\neq l'} \ b_{ll'}\, \mathbf{p}^T(\mathbf{c}_{ll'}\mathbf{c}_{ll'}^H)\mathbf{p}$ is the maximum of finitely many convex costs, and is again convex. Hence, we conclude that (12), which determines the optimal power distribution, is a convex optimization. (12) could also be reformulated as

$$\mathbf{p}_{\text{opt}} = \underset{\mathbf{p},\, t}{\text{argmin}}\ t \quad \text{s.t.} \begin{cases} \mathbf{1}_{M\times 1}^T \mathbf{p} = P_t, \\ b_{ll'}\, \mathbf{p}^T(\mathbf{c}_{ll'}\mathbf{c}_{ll'}^H)\mathbf{p} \leq t, \quad l \neq l' \in \{1,\ldots,N_g\}, \\ \mathbf{p} \geq \mathbf{0}, \\ \mathbf{p} \leq P_m. \end{cases} \tag{13}$$

which is easily solvable by convex optimization packages such as CVX [28]. It is worth mentioning that the optimal power vector $\mathbf{p}_{\text{opt}}$ does not depend on the shape of the waveforms, as long as they are pairwise orthogonal.

IV. Waveform Design

The problem of optimal power allocation among TX nodes could be viewed as a special case of waveform design, where the general shapes of the waveforms are given and we optimize the overall coherence only over the relative gains of the transmitters. Obviously, the design of the shapes, while complicates the optimization task, provides more degrees of freedom and allows for achieving lower coherence values (we will show this using a simulation in Section V). Thus, in setups without strict constraints on the waveforms, the design and optimization of the waveforms could be helpful (in some setups, due to certain requirements such the required resolution in the range/Doppler domains, there might be restrictions on the waveforms that prevent us from optimizing the waveforms; in such cases, the optimal power allocation is the only solution to improve the performance).

In [2], by defining $\mathbf{x}_{LM\times 1} = \text{vec}(\mathbf{X}^T)$, the following optimization is proposed to find the waveforms (columns of $\mathbf{X}$):

$$\mathbf{x}_{\text{opt}} = \underset{\mathbf{x}}{\text{argmin}} \sum_{l\neq l'} |\mathbf{u}_{l'}^H \mathbf{u}_l|^2 + \sum_l |\mathbf{u}_l^H \mathbf{u}_l - P_t N|^2 \quad \text{s.t.} \quad \mathbf{x}^H\mathbf{x} = P_t. \tag{14}$$

Again, $\mathbf{u}_i$s are the columns of $\mathbf{\Psi}$ that implicitly depend on $\mathbf{x}$, and P_t is the total power budget. In fact, the first term in the above cost penalizes the inner-product among different columns of $\mathbf{\Psi}$, while the second term tries to maintain the norm of all the columns close to $\sqrt{P_t N}$. The rationale for this choice of the norm comes from the previous results in the power allocation scenario with the extra orthogonality assumption on $\mathbf{X}$ columns (which is likely to be violated here). In addition, the cost function in (14) is not necessarily convex, and the proposed method in [2] is an iterative method where a convex optimization problem is solved in each of its iterations; So, it requires considerable amount of time to converge.

In this section, we focus on the waveform design challenge with a different strategy. We first demonstrate that the coherence is ruled by the covariance matrix $\mathbf{X}^H\mathbf{X}$ of the TX waveforms. For instance, the orthogonality assumption that was used in the previous section, restricts the covariance matrix to be diagonal (this assumption is no longer required in this section). Next, we devise a two-step approach: in Section IV-A, we search for the optimal covariance matrix $\mathbf{R} \triangleq \mathbf{X}^H\mathbf{X}$. In particular, we introduce three convex programs to determine $\mathbf{R}$. We continue the design in Section IV-B by finding a set of waveforms that generate the desired covariance matrix achieved in Section IV-A. This operation is not one-to-one and multiple sets of waveforms exist. Indeed, we benefit from this fact by imposing more constraints to obtain a practical optimal set.

A. Designing the Covariance Matrix of the Waveforms

In Section III, to study the optimal distribution of power, we assumed that $\mathbf{X}$ has unit-norm columns and included a diagonal matrix $\widehat{\mathbf{p}}$ (or $\mathbf{p}$) to represent the relative gain of the waveforms. In this section, however, we drop $\widehat{\mathbf{p}}$ and consider a single $\mathbf{X}$ without the unit-norm assumption. With this change, the lth column of $\mathbf{\Psi}$ in (7) can be rewritten as

$$\mathbf{u}_l = \mathbf{b}(\gamma_l) \otimes (\mathbf{X}\, \mathbf{a}(\gamma_l)). \tag{15}$$

For the sake of simplicity, from now on we denote $\mathbf{a}(\gamma_l)$ and $\mathbf{b}(\gamma_l)$ by $\mathbf{a}_l$ and $\mathbf{b}_l$, respectively. With the new notation and some properties of the Kronecker product, we can simplify the inner product of $\mathbf{u}_l$s as

$$|\mathbf{u}_{l'}^H \mathbf{u}_l|^2 = b_{ll'} \left|\mathbf{a}_{l'}^H \mathbf{X}^H \mathbf{X} \mathbf{a}_l\right|^2, \tag{16}$$

where $b_{ll'}$ was defined in (9). As claimed earlier, (16) can be expressed in term of $\mathbf{R} = \mathbf{X}^H\mathbf{X}$ in the form

$$|\mathbf{u}_{l'}^H \mathbf{u}_l|^2 = b_{ll'} |\text{Tr}\{\mathbf{A}_{ll'}\mathbf{R}\}|^2, \tag{17}$$

where $\mathbf{A}_{ll'} = \mathbf{a}_l \mathbf{a}_{l'}^H$. Also, note that the total power budget is given by $\text{Tr}\{\mathbf{R}\} = P_t$. To determine an optimal $\mathbf{R}$, we now introduce our first convex program inline with the approach of [2].

Program 1 (P. 1):

$$\mathbf{R}_{\text{opt}} = \underset{\mathbf{R}}{\text{argmin}} \sum_{l\neq l'} b_{ll'} |\text{Tr}\{\mathbf{A}_{ll'}\mathbf{R}\}|^2 + N^2 \sum_l |\text{Tr}\{\mathbf{A}_{ll}\mathbf{R}\} - P_t|^2 \quad \text{s.t.} \quad \text{Tr}\{\mathbf{R}\} = P_t, \quad \mathbf{R} \geq 0. \tag{18}$$

The cost function in P. 1 is the same as (14); we have only used the identity $b_{ll} = N^2$ and included the positivity (positive-semidefinite) constraint on $\mathbf{R}$. One can check that

the cost function in P. 1 is quadratic and convex in terms of $\mathbf{R}$ (due to the squared sums of affine forms), and the constraints are convex. Thus, P. 1 is a convex program that can be solved using packages such as CVX [28].

As (18) shows, P. 1 simultaneously aims at minimizing the cross correlation between different columns of $\mathbf{\Psi}$ and keeping the norm of each column close to $\sqrt{P_t N}$. In our second approach, we drop the column-norm penalty from the cost function and include it as a constraint to enforce exact norm equality among the columns.

Program 2 (P. 2):

$$\mathbf{R}_{\text{opt}} = \underset{\mathbf{R}}{\operatorname{argmin}} \sum_{l \neq l'} \sqrt{b_{ll'}} |\operatorname{Tr}\{\mathbf{A}_{ll'}\mathbf{R}\}| \quad \text{s.t.} \begin{cases} \operatorname{Tr}\{\mathbf{R}\} = P_t, \\ \mathbf{R} \geq 0, \\ \operatorname{Tr}\{\mathbf{A}_{ll}\mathbf{R}\} = P_t, \quad l = 1, \ldots, N_g. \end{cases} \tag{19}$$

Please note that the cost in P. 2 slightly differs from P. 1 as it involves the ℓ_1-norm of the values $\left\{\operatorname{Tr}\{\mathbf{A}_{ll'}\mathbf{R}\}\right\}_{l,l'}$ (P. 1 employs the ℓ_2-norm). Nevertheless, since ℓ_1-norm is a valid norm, the cost in P. 2 is also convex, and P. 2 is again a convex program.

As explained earlier, (14), P. 1, and P. 2, all indirectly minimize the coherence of $\mathbf{\Psi}$. In our last approach, we directly minimize the coherence. For this purpose, we need to express the coherence value in terms of $\mathbf{R}$:

$$\mu(\mathbf{\Psi}) = \max_{l \neq l'} \frac{\sqrt{b_{ll'}} |\operatorname{Tr}\{\mathbf{A}_{ll'}\mathbf{R}\}|}{N\sqrt{\operatorname{Tr}\{\mathbf{A}_{ll}\mathbf{R}\}\operatorname{Tr}\{\mathbf{A}_{l'l'}\mathbf{R}\}}}, \tag{20}$$

where we have employed (17). The above expression of the coherence, because of the denominator, is not convex in terms of $\mathbf{R}$. However, if we constrain the sensing matrix $\mathbf{\Psi}$ to have equi-norm columns (i. e. $\operatorname{Tr}\{\mathbf{A}_{ll}\mathbf{R}\} = P_t, \quad \forall l = 1, \ldots, N_g$), then, we can formulate the following convex minimization:

$$\min_{\mathbf{R}} \max_{l \neq l'} \sqrt{b_{ll'}} |\operatorname{Tr}\{\mathbf{A}_{ll'}\mathbf{R}\}| \quad \text{s.t.} \begin{cases} \operatorname{Tr}\{\mathbf{R}\} = P_t, \\ \mathbf{R} \geq 0, \\ \operatorname{Tr}\{\mathbf{A}_{ll}\mathbf{R}\} = P_t, \quad l = 1, \ldots, N_g. \end{cases} \tag{21}$$

The above minimization can be reformulated as a standard convex program in the following form:

Program 3 (P. 3):

$$\mathbf{R}_{\text{opt}} = \underset{t, \mathbf{R}}{\operatorname{argmin}}\ t \quad \text{s.t.} \begin{cases} \operatorname{Tr}\{\mathbf{R}\} = P_t, \\ \mathbf{R} \geq 0, \\ \sqrt{b_{ll'}} |\operatorname{Tr}\{\mathbf{A}_{ll'}\mathbf{R}\}| \leq t, \quad l \neq l' \in \{1, \ldots, N_g\}, \\ \operatorname{Tr}\{\mathbf{A}_{ll}\mathbf{R}\} = P_t, \quad l = 1, \ldots, N_g. \end{cases} \tag{22}$$

Similar to the power allocation program (13), we can impose per antenna maximum power constraints in each of P. 1 to P. 3 waveform design programs as:

$$[\mathbf{R}]_{i,i} \leq P_m, \quad i = 1, 2, \ldots, M \tag{23}$$

Including these constraints could be beneficial in comparing the performance/computational-cost of the power allocation and the waveform design programs. In particular, we apply these constraints only in one of our experiments in Section V (Fig. 6) to provide a fair comparison between the two programs. Nevertheless, we exclude these constraints in other experiments to simplify the waveform design process.

B. Signal Synthesis

Our three programs in Section IV-A determine a valid covariance matrix $\mathbf{R}$. In this section, we shall determine a set of waveforms whose covariance matrix equals or nearly equals $\mathbf{R}$.

Note that the constraint $\mathbf{R} > 0$, which implies that $\mathbf{R}_{M \times M}$ is non-negative-definite, exists in all of the proposed methods. This property confirms that $\mathbf{R}^{1/2}$ exists and is well-defined. Now, it is well-known that any matrix $\mathbf{X}_{L \times M}$ that satisfies $\mathbf{X}^H\mathbf{X} = \mathbf{R}$ can be written as

$$\mathbf{X} = \mathbf{U}\mathbf{R}^{1/2}, \tag{24}$$

where $\mathbf{U}_{L \times M}$ is a semi-unitary matrix ($\mathbf{U}^H\mathbf{U} = \mathbf{I}$). This reveals that there is no unique set of optimal waveforms. Fortunately, all possible optimal sets are known through $\mathbf{U}_{L \times M}$. This enables us to determine $\mathbf{U}_{L \times M}$ in such a way that the resulting waveforms benefit from additional useful properties. An incomplete list of practical considerations include small PAPR values [33], [34], constant modulus waveforms [9], [13], similarity of the waveforms to a given set with desired ambiguity features [35], [36], and a combination of such consraints [11], [37]–[39]. Here we focus on the constant modulus property as the design constraint. In fact, waveforms with constant modulus are necessary when the radar amplifiers work in the saturation mode. The problem of synthesizing the waveform matrix with almost-constant-modulus constraint can be formulated as:

$$\min_{\mathbf{X}, \mathbf{U}} \|\mathbf{X} - \mathbf{U}\mathbf{R}^{1/2}\|^2 \quad \text{s.t.} \begin{cases} \mathbf{U}^H\mathbf{U} = \mathbf{I} \\ |x_m(l)| = \sqrt{\frac{r_{mm}}{L}} \quad \substack{1 \leq m \leq M \\ 1 \leq l \leq L} \end{cases} \tag{25}$$

where r_{mm} is the mth diagonal element of $\mathbf{R}$.

To find the minimizer of (25), an iterative method is proposed in [10]. In this approach, matrices $\mathbf{X}$ and $\mathbf{U}$ are alternatively updated. In other words, after initializing the method, at each iteration, one of $\mathbf{X}$ and $\mathbf{U}$ are kept constant, while the other one is tuned to maximally decrease the cost value. The details and convergence analysis of this technique are studied in [10]. It should be highlighted that the stage-wise minimizations have closed-forms and are computationally affordable. If we denote the final matrices found with this technique by $\widehat{\mathbf{X}}$ and $\widehat{\mathbf{U}}$, then, $\widehat{\mathbf{X}}$ does not necessarily regenerate $\mathbf{R}$ in the exact form. Now, there are two options: 1) either we adopt $\widehat{\mathbf{U}}\mathbf{R}^{1/2}$ with small PAPR-valued waveforms that exactly generate the covariance matrix $\mathbf{R}$, or 2) directly employ the obtained waveform matrix $\widehat{\mathbf{X}}$ that consists of constant modulus waveforms that approximately generate the covariance matrix

R (degradation of the performance). In our experiments, we observed that the latter degradation is rather negligible and could be ignored. Therefore, we adopt the second approach that ensures waveforms with constant modulus.

V. Performance Analysis

We consider a colocated MIMO configuration in which TX and RX nodes are randomly located on a small disk of radius $r_d = 10\,m$ following a uniform distribution both for their ranges and their angles. Moreover, carrier frequency is $f = 5\,\text{GHz}$ and NESTA method is employed for CS recovery [32]. Our main focus is to evaluate the CS-based multi-target detection performance of the proposed schemes of power allocation and waveform design for this radar. Specifically, using numerical simulation, we obtain plots of probability of detection P_d versus signal-to-noise ratio (SNR) at a given probability of false alarm P_{fa}. Before we proceed to the simulation results, which will be given in two separate parts for power allocation and waveform design, we discuss about choosing the angular grid that impacts the columns of the sensing matrix in (6).

Since we estimate the azimuth angle in our radar, each target could be located at any angle between 0° to 360°. In our CS-based radar, however, this angular range is replaced with a uniform grid; *i.e.*, the continuum of angles is represented via finitely many grid points. In this scenario, the location of each target is rounded to its nearest grid point. Obviously, the angular resolution r_γ (the distance between two adjacent angular grid points) potentially describe the accuracy of the system. Unfortunately, by increasing the resolution of the angular grid (decreasing r_γ), we do not necessarily improve the accuracy of the radar. To illustrate this fact, we present a simulation scenario with $M_t = 20$ transmitters and $N_r = 20$ receivers. The TX/RX nodes are randomly placed inside a disk of radius r_d with uniform distribution. This implies that the aperture of the radar is limited to $2r_d$ (the aperture of the resulting virtual array is about $4r_d$). Further, we consider orthogonal Hadamard sequences for the transmitting waveforms and uniform power allocation. To study the role of angular resolution r_γ in the overall performance, we consider two equi-size targets at angles 0° and r_γ with independent phases (uniformly distributed from 0° to 360°). Finally, we attempt to estimate the targets from the gathered measurements in a high SNR situation ($\text{SNR} = 30\text{dB}$ where SNR is defined as $1/\sigma^2$) using the NESTA sparse recovery method. In each run, if the location of two largest elements of the recovered vector (using NESTA) coincides with the original location of targets, we count this detection as successful. For each value of r_γ, we perform 1000 trials with independent realizations for the placement of TX/RX nodes. The percentage of successful detection is reported as the rate of correct support estimation in Fig. 1. This figure reveals that for each r_d, the rate of success starts to degrade below a certain level of r_γ. In other words, although the angular resolution of the grid is improved, the recovery method is not able to properly resolve the two adjacent targets. For instance, with $r_d = 10m$, the additional computational costs for r_γ below 0.1° is not justifiable. Thus,

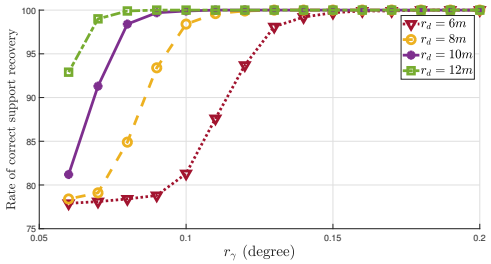

Fig. 1: Rate of correct support estimation vs. angular resolution (r_γ).

we fix $r_\gamma = 0.1^\circ$ in this case (and in our simulations for performance evaluation of the proposed methods). Another observation from Fig. 1 is that as expected, the angular resolution is inversely proportional to the aperture size r_d; the rate of success is roughly a function of $r_\gamma\, r_d$. It should be mentioned that by adopting an angular grid in a CS-based scenario, targets that lie in the same bin of the grid are detected as a single target with the overall reflection coefficient. Also, the extent of the grid can be potentially from 0° to 360°. However, there might be some prior information on possible angles of arrival of targets. In such cases, the extent of the grid can be confined. Another case is when the TX/RX antennas are not omnidirectional and illuminate only a portion of azimuth angles. In our simulations, we consider a confined range of angles for performance evaluation to keep the computational complexity low.

A. Power Allocation

In this section, an azimuth angle grid $[-15^\circ, -14.9^\circ, \ldots, 14.9^\circ, 15^\circ]$ is considered. Orthogonal Hadamard sequences with $L = 32$ are employed as the transmitted waveforms (with unit norm). The total power P_t is set equal to the number of transmiters M and maximum power for each TX antenna is set to $P_m = 8W$. Then, the optimtal powers of the transmitters are obtained by solving (13) using CVX package. We also compute the powers using the method proposed in [2] in which a sum of squared inner products of all the cross columns in the sensing matrix is minimized. To obtain the plots of P_d vs SNR for a probability of false alarm $P_{fa} = 10^{-4}$, a Monte Carlo simulation is conducted with 20000 independent runs. In each run, three targets are generated on the considered grid with reflection coefficients β_ks coming from a complex Gaussian distribution with zero mean and covarince matrix $\Sigma_\beta = \frac{1}{2}\mathbf{I}_{2\times 2}$ ($E\{|\beta_k|^2\} = 1$). This is the case in the traditional Swerling case I model which yields exponentially distributed RCS values [40]. Locations of the generated targets on the grid are also determined randomly. Received signals at the receivers are corrupted by zero mean complex Gaussian noise with variance σ^2 and SNR is defined as $1/\sigma^2$. After recovery of the sparse target scene using NESTA, we compare the resulting values associated with angular bins against a threshold to detect the targets. The value of this threshold is determined such that the probability P_{fa} of false alarm (defined as the percentage of the bins with values above the threshold that actually contain no targets) achieves a given

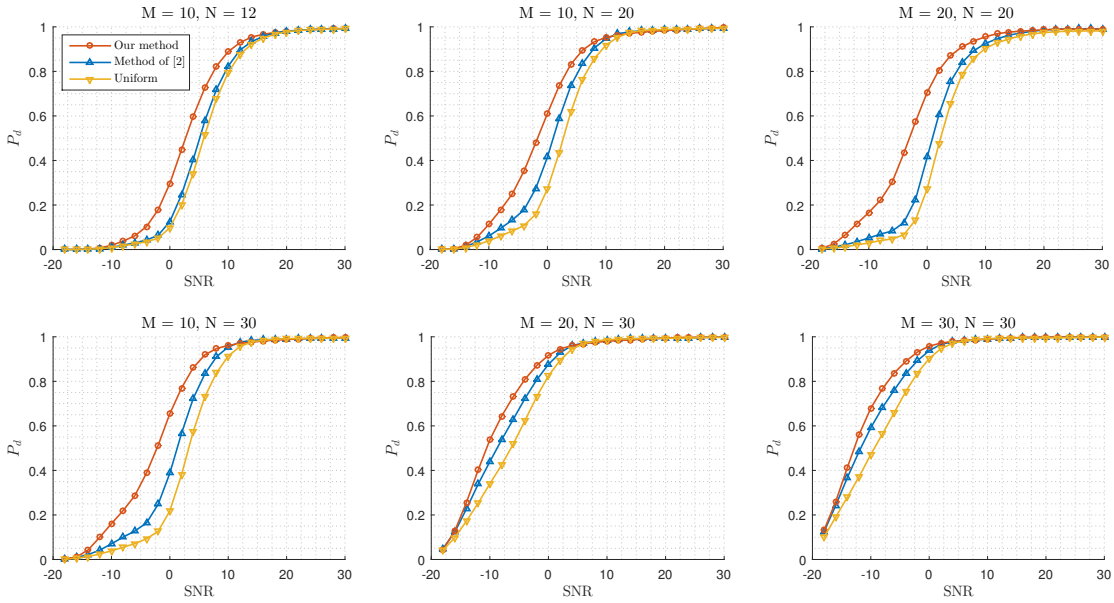

Fig. 2: P_d vs. SNR for different power allocation methods, $P_{fa} = 10^{-4}$, $L = 32$.

value (here 10^{-4}). Then, P_d is defined as the percentage of runs (among the total 200000 trials) in which all the three targets are correctly detected. The curves of P_d versus SNR for 6 different configurations and different parameters have been shown in Fig. 2 for our proposed method, the method proposed in [2], and the uniform power allocation. As can be seen from the curves, our proposed method outperforms all the other methods in all the configurations.

B. Waveform Design

Here, before we proceed to performance evaluation of the proposed methods, it should be noted that the most relevant waveform design technique to the ones considered in this paper is the method of [2]. Therefore, it is desirable to compare our results with this method. However, the iterative procedure presented in [2] is rather slow and computationally complex. Furthermore, our P. 1 method essentially performs the same task with a different setting. Ideally, the two methods (P. 1 and the method of [2]) shall perform equally. However, due to finite numerical precision and stopping conditions of the iterative methods, they are not identical. To compare the performance of P. 1 and the method of [2], we perform two simple tests using $(L, M, N) = (8, 6, 6)$ and $(L, M, N) = (16, 8, 8)$. In both tests, we randomly generate the location of TX and RX nodes in 50 different trials and run both P. 1 and the method proposed in [2] in each trial. We also apply the signal synthesis procedure of Section IV-B to the covariance matrix found by P. 1 which results in constant modulus waveforms. In Fig. 3, we have plotted the final cost values of the waveforms obtained using the method of [2], covariance matrices obtained by P. 1, and the P. 1 method followed by the constant modulus signal synthesis (P. 1 + signal synthesis) in each of the trials. Notice that the increase in cost due to signal synthesis procedure is so small that could be neglected. Moreover, although both the method of [2] and P. 1 aim at minimizing the same cost, we observe that P. 1 consistently achieves lower cost values (around 10%). On average, P. 1 stops at cost values 10% less than the method of [2] (horizontal lines). The main advantage of P. 1 is, however, its speed. Indeed, the method of [2] is an iterative method that minimizes a convex cost in each iteration (actually, it requires many iterations to reach the solution). As a comparison, we performed a test on our platform with Intel Core (TM) i7-3610QM, 2.30 GHz and 12.0 GB of memory using $L = 32$ and $M = N$ and an azimuth grid as $[-4°, -3.6°, \ldots, 3.2°, 4°]$ (we consider a small and undersampled grid to not exceed the available memory on our platform while running the method of [2] and to reduce the total simulation time). In Fig. 4, we have plotted the run times for our proposed methods P. 1 - P. 3 followed by the signal synthesis process along with the run times of only one iteration of the method of [2]. The results suggest that the proposed methods (and in particular P. 1, which performs the same task as the method of [2]) are much faster than the method of [2].

With these two observations regarding P.1 and the method of [2] (lower cost values and computation time of P. 1), we no longer include the exact method of [2] in our following tests for detection performance evaluation, and only consider its alternative P. 1.

To obtain performance curves, here we consider a smaller azimuth grid as $[-4°, -3.9°, \ldots, 3.9°, 4°]$. The reason for this choice is to compensate for the high computational complexity due to the larger size of the waveform design programs than the ones in the power allocation. Firstly, we obtain optimal waveform covariance matrices by solving each of the three programs introduced in Section IV-A. Then, using the method introduced in section IV-B, constant modulus

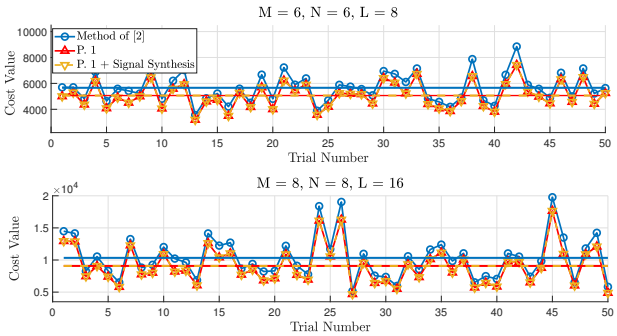

Fig. 3: Comparison of the obtained cost function values using the waveform design method of [2], P. 1, and P. 1 + signal synthesis. Average values have been shown by straight lines.

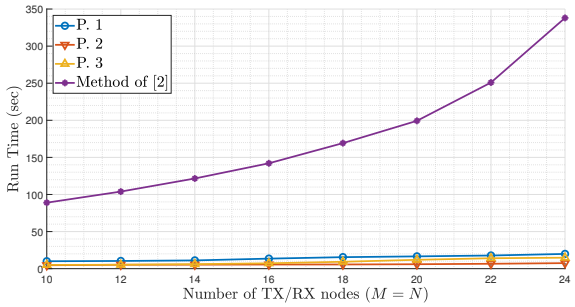

Fig. 4: Run Time vs. the number of TX/RX nodes for different methods. For the method of [2] we plotted the run times of only one iteration of the algorithm. Run times for P. 1 - P. 3 also include the signal synthesis process.

signals are achieved for each waveform covariance matrix. Now sensing matrices for different methods are determined and the Monte Carlo simulation with the same details as in the Section V-A can be conducted to obtain curves of P_d vs SNR for $P_{fa} = 10^{-4}$. The obtained curves for 4 different scenarios have been shown in Fig. 5, where along the waveforms obtained from the proposed programs, the Hadamard waveforms are also considered. The results indicate that the waveforms related to P. 3 (exact minimization of the coherence) consistently outperform other methods. At low to moderate number of transmitters, the waveforms obtained from P. 1 and P. 2 exhibit almost the same performance but slightly better than that of the Hadamard waveform. However, when the number of transmitters increases, the curve of P. 1 start to overtake that of P. 2. Finally, since our P. 3 method (followed by the signal synthesis) consistently outperforms other methods, and does not impose more computational cost (as observed in Fig. 4), we identify P. 3 as our proposed choice of the waveform design for CS-based MIMO radar.

Our last experiment is designed to compare the power allocation and waveform design methods in terms of the achieved coherence value (which controls the overall CS-based detection performance) and the run time. For the power allocation program, we use (13) with Hadamard waveforms. For the waveform design, we use P. 3 with the additional per antenna maximum power constraints as stated in (23) (direct minimization of coherence is approached in both considered programs). We also include the results for synthesized constant modulus waveforms. We use $M = N$, $L = 32$, and the azimuth grid as $[-4^\circ, -3.9^\circ, \ldots, 3.9^\circ, 4^\circ]$. In Fig. 6a, we depict the run time of each method for various values of M. Unlike the waveform design, the computational cost of the power allocation program is not much influenced by the increase in M in the considered range. In addition, the power allocation program is consistently faster than the waveform design procedure. In fact, the size of the optimization problem grows quadratically with M in the waveform design problem, while it remains linear with M in the power allocation problem. Another observation is that the contribution of signal synthesis process in the run time for the constant modulus waveforms is marginal. The achieved coherence values are also plotted in Fig. 6b. As expected, the waveform design consistently outperforms the power allocation program by providing lower coherence values. If the waveforms in the waveform design problem had been constrained to be orthogonal, then, the off-diagonal elements of $\mathbf{R}$ would have vanished (what would remained were the diagonal elements which indeed represent the transmitting powers). This meant that the two methods of waveform design and power allocation would result in the same covariance matrix, and consequently, the same coherence value (note that the orthogonality constraint also ensures $\mathrm{Tr}\{\mathbf{A}_{ll}\mathbf{R}\} = P_t$ in the waveform design program; however, the reverse is not true). Thus, the superiority of the curve of the waveform design method in Fig. 6b, indicates that the obtained optimal waveforms are not orthogonal, yet, they perform better than an orthogonal set with the same power constraints. As expected, the coherence values associated with constant modulus waveforms are slightly more than the ones obtained with the optimized covariance matrix, however, the increase is not considerable. In applications where this slight increase is not acceptable, one can opt for waveforms with low PAPR (instead of constant modulus) that coincide with the optimal covariance matrix (as explained in Section IV-B).

In summary, Fig. 6 shows a trade-off between the computational complexity and the performance in using the two methods. However, the required computations in the two methods could be considered as an offline preprocessing part in most scenarios. This fact downgrades the role of the computational cost, and identifies the waveform design as the superior approach, whenever feasible.

VI. Conclusion

Improvement of the multi-target detection capability of a CS-based colocated MIMO radar with given location (random placement) of TX/RX antennas was investigated in this paper through power allocation and waveform design. Our approach was based on reduction of the coherence of the sensing matrix to improve the CS-based detection. For power allocation, adopting a set of orthogonal transmitted waveforms, we derived a convex optimization program to minimize the coherence of the resulting sensing matrix (subjected to total power and maximum per antenna power constraints). Simulation results showed that our proposed method outperforms the method proposed in [2] and the uniform power allocation from the viewpoint of multi-target detection quality. For the waveform design, we demonstrated the sole dependency of coherence measures on the covariance matrix of the transmitting

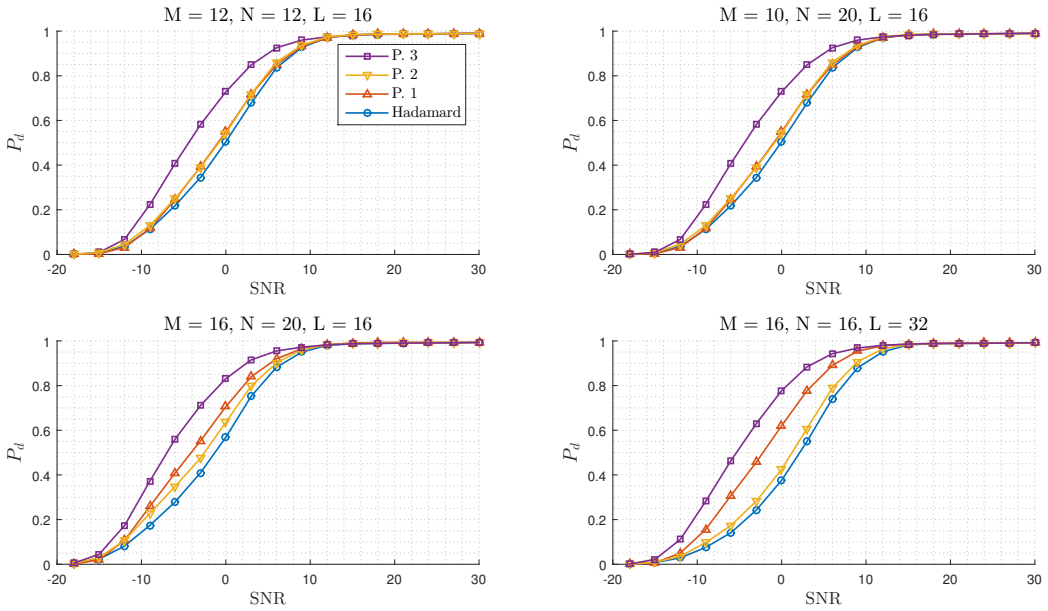

Fig. 5: P_d vs SNR for different waveform design methods, $P_{fa} = 10^{-4}$.

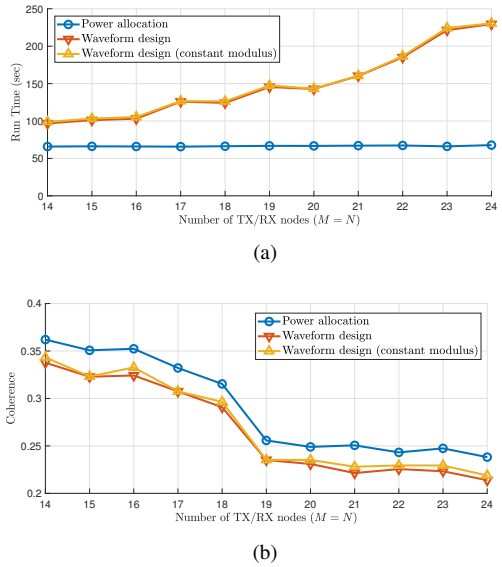

(a)

(b)

Fig. 6: Comparison of power allocation and waveform design for (a) run time and (b) coherence measure.

signals and aimed at designing this covariance matrix rather than the waveforms themselves. Then, due to existence of infinitely many solutions for transforming a covaraince matrix into a set of waveforms, we were able to also consider some practical constraints on the waveforms while transforming from the covariance matrix. Specifically, intending to reduce the coherence, we derived and solved three different convex programs (P. 1, P. 2, and P. 3) for achieving the covariance matrix. Then, we followed the method proposed in [10] to obtain constant modulus waveforms. Unlike the method of [2] in which waveforms are designed directly using an iterative algorithm, our two-step strategy not only reduces the computation time but also ensures some practical constraints for the waveforms. Simulation results showed that the method based on P. 3 in which the mutual coherence is minimized directly presents better detection performance compared to the others. We also conducted a simulation to compare power allocation with waveform design which showed the trade-off between performance and complexity in using the two procedures. To make this comparison possible, we derived and considered a per antenna maximum power constraint in the waveform design program.

REFERENCES

[1] A. Ajorloo, A. Amini, and M. H. Bastani, "An approach to power allocation in MIMO radar with sparse modeling for coherence minimization," in *2017 25th European Signal Processing Conference (EUSIPCO)*, Aug 2017, pp. 1927–1931.

[2] Y. Yu, S. Sun, R. N. Madan, and A. Petropulu, "Power allocation and waveform design for the compressive sensing based MIMO radar," *IEEE Transactions on Aerospace and Electronic Systems*, vol. 50, no. 2, pp. 898–909, 2014.

[3] E. Fishler, A. Haimovich, R. Blum, D. Chizhik, L. Cimini, and R. Valenzuela, "MIMO radar: An idea whose time has come," in *Radar Conference, 2004. Proceedings of the IEEE.* IEEE, 2004, pp. 71–78.

[4] A. M. Haimovich, R. S. Blum, and L. J. Cimini, "MIMO radar with widely separated antennas," *IEEE Signal Processing Magazine*, vol. 25, no. 1, pp. 116–129, 2008.

[5] J. Li and P. Stoica, "MIMO radar with colocated antennas," *IEEE Signal Processing Magazine*, vol. 24, no. 5, pp. 106–114, 2007.

[6] J. Li, P. Stoica, L. Xu, and W. Roberts, "On parameter identifiability of MIMO radar," *IEEE Signal Processing Letters*, vol. 14, no. 12, pp. 968–971, 2007.

[7] P. Stoica, J. Li, and Y. Xie, "On probing signal design for MIMO radar," *IEEE Transactions on Signal Processing*, vol. 55, no. 8, pp. 4151–4161, 2007.

[8] Y. Yang and R. S. Blum, "MIMO radar waveform design based on mutual information and minimum mean-square error estimation," *IEEE Transactions on Aerospace and Electronic Systems*, vol. 43, no. 1, 2007.

[9] D. R. Fuhrmann and G. San Antonio, "Transmit beamforming for MIMO radar systems using signal cross-correlation," *IEEE Transactions on Aerospace and Electronic Systems*, vol. 44, no. 1, 2008.

[10] P. Stoica, J. Li, and X. Zhu, "Waveform synthesis for diversity-based transmit beampattern design," *IEEE Transactions on Signal Processing*, vol. 56, no. 6, pp. 2593–2598, 2008.

[11] G. Cui, H. Li, and M. Rangaswamy, "MIMO radar waveform design with constant modulus and similarity constraints," *IEEE Transactions on Signal Processing*, vol. 62, no. 2, pp. 343–353, 2014.
[12] Z. Lin and Z. Wang, "Interleaved OFDM signals for MIMO radar," *IEEE Sensors Journal*, vol. 15, no. 11, pp. 6294–6305, 2015.
[13] O. Aldayel, V. Monga, and M. Rangaswamy, "Tractable transmit MIMO beampattern design under a constant modulus constraint," *IEEE Transactions on Signal Processing*, 2017.
[14] Y. Yu, A. P. Petropulu, and H. V. Poor, "Compressive sensing for MIMO radar," in *Acoustics, Speech and Signal Processing, 2009. ICASSP 2009. IEEE International Conference on*. IEEE, 2009, pp. 3017–3020.
[15] ——, "MIMO radar using compressive sampling," *IEEE Journal of Selected Topics in Signal Processing*, vol. 4, no. 1, pp. 146–163, 2010.
[16] C.-Y. Chen and P. Vaidyanathan, "Compressed sensing in MIMO radar," in *2008 42nd Asilomar Conference on Signals, Systems and Computers*. IEEE, 2008, pp. 41–44.
[17] T. Strohmer and B. Friedlander, "Compressed sensing for MIMO radar-algorithms and performance," in *Signals, Systems and Computers, 2009 Conference Record of the Forty-Third Asilomar Conference on*. IEEE, 2009, pp. 464–468.
[18] A. P. Petropulu, Y. Yu, and J. Huang, "On exploring sparsity in widely separated MIMO radar," in *Signals, Systems and Computers (ASILOMAR), 2011 Conference Record of the Forty Fifth Asilomar Conference on*. IEEE, 2011, pp. 1496–1500.
[19] S. Gogineni and A. Nehorai, "Target estimation using sparse modeling for distributed MIMO radar," *IEEE Transactions on Signal Processing*, vol. 59, no. 11, pp. 5315–5325, 2011.
[20] B. Li and A. P. Petropulu, "Distributed MIMO radar based on sparse sensing: Analysis and efficient implementation," *IEEE Transactions on Aerospace and Electronic Systems*, vol. 51, no. 4, pp. 3055–3070, 2015.
[21] E. J. Candes, "The restricted isometry property and its implications for compressed sensing," *Comptes Rendus Mathematique*, vol. 346, no. 9-10, pp. 589–592, 2008.
[22] A. Amini and F. Marvasti, "Deterministic construction of binary, bipolar and ternary compressed sensing matrices," *IEEE Transaction on Information Theory*, vol. 57, no. 4, pp. 2360–2370, 2011.
[23] J. Zhang, D. Zhu, and G. Zhang, "Adaptive compressed sensing radar oriented toward cognitive detection in dynamic sparse target scene," *IEEE Transactions on Signal Processing*, vol. 60, no. 4, pp. 1718–1729, 2012.
[24] H. Hu, M. Soltanalian, P. Stoica, and X. Zhu, "Locating the few: Sparsity-aware waveform design for active radar," *IEEE Transactions on Signal Processing*, vol. 65, no. 3, pp. 651–662, 2017.
[25] S. Gogineni and A. Nehorai, "Frequency-hopping code design for MIMO radar estimation using sparse modeling," *IEEE Transactions on Signal Processing*, vol. 60, no. 6, pp. 3022–3035, 2012.
[26] N. S. Subotic, B. Thelen, K. Cooper, W. Buller, J. Parker, J. Browning, and H. Beyer, "Distributed radar waveform design based on compressive sensing considerations," in *Radar Conference, 2008. RADAR'08. IEEE*. IEEE, 2008, pp. 1–6.
[27] H. Liu, X. Wang, B. Jiu, J. Yan, M. Wu, and Z. Bao, "Wideband MIMO radar waveform design for multiple target imaging," *IEEE Sensors Journal*, vol. 16, no. 23, pp. 8545–8556, 2016.
[28] M. Grant and S. Boyd, "CVX: MATLAB software for disciplined convex programming."
[29] S. S. Chen, D. L. Donoho, and M. A. Saunders, "Atomic decomposition by basis pursuit," *SIAM review*, vol. 43, no. 1, pp. 129–159, 2001.
[30] J. A. Tropp and A. C. Gilbert, "Signal recovery from random measurements via orthogonal matching pursuit," *IEEE Transactions on information theory*, vol. 53, no. 12, pp. 4655–4666, 2007.
[31] E. Candes and T. Tao, "The dantzig selector: Statistical estimation when p is much larger than n," *The Annals of Statistics*, pp. 2313–2351, 2007.
[32] S. Becker, J. Bobin, and E. J. Candès, "NESTA: A fast and accurate first-order method for sparse recovery," *SIAM Journal on Imaging Sciences*, vol. 4, no. 1, pp. 1–39, 2011.
[33] A. De Maio, Y. Huang, M. Piezzo, S. Zhang, and A. Farina, "Design of optimized radar codes with a peak to average power ratio constraint," *IEEE Transactions on Signal Processing*, vol. 59, no. 6, pp. 2683–2697, 2011.
[34] S. Sen, "Characterizations of PAPR-constrained radar waveforms for optimal target detection," *IEEE Sensors Journal*, vol. 14, no. 5, pp. 1647–1654, 2014.
[35] A. De Maio, S. De Nicola, Y. Huang, S. Zhang, and A. Farina, "Code design to optimize radar detection performance under accuracy and similarity constraints," *IEEE Transactions on Signal Processing*, vol. 56, no. 11, pp. 5618–5629, 2008.
[36] A. De Maio, S. De Nicola, Y. Huang, Z.-Q. Luo, and S. Zhang, "Design of phase codes for radar performance optimization with a similarity constraint," *IEEE Transactions on Signal Processing*, vol. 57, no. 2, pp. 610–621, 2009.
[37] S. M. Karbasi, A. Aubry, V. Carotenuto, M. M. Naghsh, and M. H. Bastani, "Knowledge-based design of space–time transmit code and receive filter for a multiple-input–multiple-output radar in signal-dependent interference," *IET Radar, Sonar & Navigation*, vol. 9, no. 8, pp. 1124–1135, 2015.
[38] B. Tang and J. Tang, "Joint design of transmit waveforms and receive filters for MIMO radar space-time adaptive processing," *IEEE Transactions on Signal Processing*, vol. 64, no. 18, pp. 4707–4722, 2016.
[39] J. Zhang, C. Shi, X. Qiu, and Y. Wu, "Shaping radar ambiguity function by l-phase unimodular sequence," *IEEE Sensors Journal*, vol. 16, no. 14, pp. 5648–5659, 2016.
[40] M. I. Skolnik, *Introduction to Radar Systems*, 3rd ed. New York: McGraw Hill Book Co., 2001.

Abdollah Ajorloo was born in Tehran, Iran. He received his B.Sc. from Shahed University, Tehran, Iran in 2011 and his M.Sc. from Sharif University of Technology, Tehran, Iran in 2013, both in Electrical Engineering. He is currently pursuing his Ph.D. in Electrical Engineering at Sharif University of Technology. His research interests include statistical signal processing, compressed sensing, and MIMO radar.

Arash Amini received B.Sc., M.Sc., and Ph.D. degrees in Electrical Engineering (Communications and Signal Processing), in 2005, 2007, and 2011, respectively, and the B.Sc. degree in Petroleum Engineering (Reservoir), in 2005, all from Sharif University of Technology (SUT), Tehran, Iran. He was a researcher at École Polytechnique Fédérale (EPFL), Lausanne, Switzerland, from 2011 to 2013, working on statistical approaches towards modeling sparsity in continuous-domain. Since September 2013, he is an Assistant Professor at Sharif University of Technology, Tehran, Iran. He is also an associate editor of IEEE Signal Processing Letters, since July 2014. His research interests include various topics in statistical signal processing, specially compressed sensing.

Mohammad Hassan Bastani received his B.Sc. degree in Electrical Engineering in 1979 from Sharif University of Technology, Tehran, Iran. He received his Dipl.-Ing. And Ph.D. degrees from École Nationale Supérieure des Télécommunications (ENST), Paris, France, in Electrical Engineering, in 1981 and 1984, respectively. He is currently an associate professor at the Department of Electrical Engineering of Sharif University of Technology. His research interests are stochastic signal processing, data fusion, and radar design.